Impact of the water-compatible periphery on the dynamic and structural properties of benzene-1,3,5-tricarboxamide based amphiphiles

Journal Name

COMMUNICATION

Impact of the water-compatible periphery on the dynamic assembly properties of benzene-1,3,5-tricarboxamide based amphiphiles†

Received 00th January 20xx,
Accepted 00th January 20xx

DOI: 10.1039/x0xx00000x

www.rsc.org/

S.M.C. Schoenmakers,[a] C.M.A. Leenders,[a] R.P.M. Lafleur, [a] X. Lou, [a] E.W. Meijer,*[a] G.M. Pavan*[b] and A.R.A. Palmans*[a]

The consequences of using saccharides versus tetra(ethyleneglycol) chains as water-compatible moieties on the morphology and dynamics of supramolecular polymers in aqueous solutions is investigated. The saccharides form many H-bonds with other saccharides within the polymer and with water, increasing the hydration of the fiber and changing its dynamics.

Saccharides are ubiquitous in Nature and fulfil important regulatory, recognition and signal transduction functions.[1] In chemistry, saccharides have been attached to covalent polymers, fatty acids, peptides, dendrimers, and a variety of nanoparticles with the aim to achieve selective and efficient interactions with saccharide-binding proteins.[2–10] In addition, saccharides attached to water-incompatible moieties impart excellent water compatibility, affording biocompatible hydrogels and surfaces.[11–13] Since molecular interactions involving saccharides are generally weak, multivalency plays an important role to increase their interaction strength. Recently, self-assembling scaffolds with peripheral saccharides have been investigated as an alternative method to create multivalent systems.[14] Such systems have the advantage of remaining responsive, guarantee easy accessibility, and permit to combine different ligands through mixing of building blocks. In addition, water-compatible supramolecular polymers attract increasing attention due to their potential as biomaterials.[15]

The responsive nature of self-assembled systems is directly linked to the dynamic exchange of monomers between different aggregates. The rate of exchange and stability of the system strongly depend on the molecular interactions encoded in the chemical structure of the monomers,[16–19] and on the interactions with the solvent.[20–22] The exchange of molecules between aggregates has been tracked by attaching bulky probe molecules to the molecule of interest,[16,17,23] but recently hydrogen-deuterium exchange (HDX) followed by mass spectrometry (MS) emerged as a powerful tool to study the exchange processes in supramolecular systems.[24]

We recently disclosed self-assembling, amphiphilic, discotic compounds based on the benzene-1,3,5-tricaboxamide unit comprising tetra(ethyleneglycol) (TEG) chains (**EG-BTA**, Scheme 1). We elucidated the importance of a sufficiently large hydrophobic spacer in amphiphilic BTA assemblies on the stability of the aggregates formed,[25] and with the help of HDX-MS we measured the dynamic exchange of monomers between aggregates in water.[24] However, reports of hypersensitivity to, and early degradation of ethyleneglycol-based materials stimulated us to explore alternative units.[26] We recently replaced the TEG chains by various monosaccharides, including D-glucopyranoside (**Glu-BTA**, Scheme 1), functioning as both a water-compatible periphery and as a biological recognition motif.[27]

In this contribution, we present a systematic comparison between supramolecular assemblies decorated with D-glucopyranosides (**Glu-BTA**) and our previously reported **EG-BTA**-based assemblies. We here study in detail the influence of the water-compatible periphery on the morphology of the assemblies and investigate if and how the nature of the periphery affects the dynamic nature of the assembly properties using a combination of molecular dynamics (MD) simulations, HDX-MS, static light scattering (SLS), UV-Vis spectroscopy and ^{1}H-NMR spectroscopy.

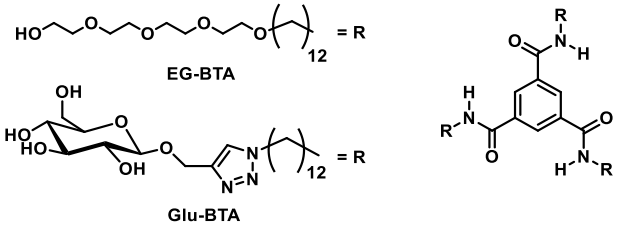

Scheme 1 Chemical structure of the investigated **EG-BTA** and **Glu-BTA**.

[a] Institute for Complex Molecular Systems, Eindhoven University of Technology, P.O. Box 513, 5600 MB Eindhoven, The Netherlands. E-mail a.palmans@tue.nl; Tel: +31 040 2473101
[b] Department of Innovative Technologies, University of Applied Sciences and Arts of Southern Switzerland, Galleria 2, Via Cantonale 2c, Manno CH-6928, CH. Email: giovanni.pavan@supsi.ch

† Electronic Supplementary Information (ESI) available: materials and methods, supporting data of UV-Vis, static light scattering experiments, small angle X-ray scattering, cryoTEM experiments, ^{1}H NMR, FT-IR and additional information about the HDX-MS and molecular dynamics experiments. See DOI: 10.1039/x0xx00000x

Please do not adjust margins

First, the morphologies of the BTA assemblies were compared. SLS and small angle X-ray scattering (Fig. S1, ESI†) both point towards the formation of anisotropic assemblies of roughly the same dimensions. Closer inspection of cryogenic transmission electron microscopy images of **EG-BTA** and **Glu-BTA** confirms that both form long, narrow fibres of micrometres in length and that the diameter is in both cases around 5 nm (Fig. 1). Apart from forming similar morphologies, the FT-IR spectra of **EG-BTA** and **Glu-BTA** in D_2O show the amide I vibration at identical positions (ν = 1634 cm^{-1}), indicative for the presence of intermolecular H-bonds between the core amides of both assemblies (Fig. S2, ESI†). These results indicate that both types of BTAs form H-bond stabilised supramolecular polymers in water.

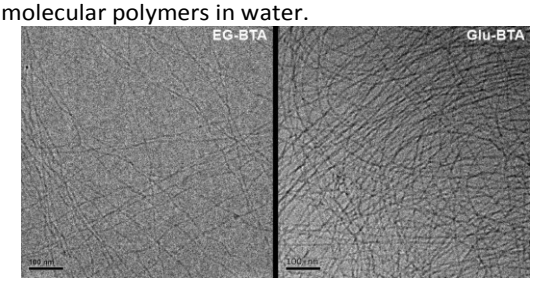

Fig. 1 CryoTEM images of **EG-BTA** (c = 0.58 mM) and **Glu-BTA** (c = 0.67 mM) in water.

Apart from similarities, the two BTA systems also show differences. The **EG-BTA** assemblies are characterized by a UV-Vis spectrum with maxima at 212 and 226 nm, while the UV-Vis spectrum of **Glu-BTA** shows a more pronounced maximum at 213 nm and a small shoulder at 225 nm (Fig. S3A, ESI†). The increased absorbance around 213 nm in the spectrum of **Glu-BTA** is attributed to the presence of the 1,2,3-triazole moiety that absorbs around the same wavelength (Fig. S3B, ESI†). In addition, upon cooling down from 90 °C to 20 °C, **Glu-BTA** shows a transition from 55 to 43 °C (Fig. S4B, ESI†) in the UV absorbance of the BTA chromophore. As expected, there is no cloud point (Fig. S4C, ESI†). For **EG-BTA**, a cloud point is observed at 72 °C (Fig. S5C, ESI†), due to the lower critical solution temperature behaviour of ethyleneglycol.[28] From 50 to 38 °C, an additional, sharp transition occurs in the UV absorbance of the BTA chromophore (Fig. S5B, ESI). Additional studies with SLS and ^{1}H-NMR at elevated temperatures suggest that the transition around 50 °C in **Glu-BTA** originates from the conversion of small aggregates into long, ordered supramolecular polymers upon cooling (Fig. S6 & S7, ESI†). The situation for **EG-BTA** is more complex: above 72 °C, very large aggregates exist due to the increased hydrophobicity of TEG at those temperatures. Also in this case, the transition observed around 50 °C originates from the conversion of disordered aggregates into long, ordered supramolecular polymers (Fig. S8 & S9, ESI†). In contrast to previously studied water-compatible BTAs that comprised either stereogenic centres in the aliphatic chains[24,25,29] or were connected to a proline derivative,[30] no CD effect was observed in case of **Glu-BTA**, indicating that no helical bias is present in these supramolecular polymers.[27] Finally, we assessed the presence of a hydrophobic pocket around the core of the BTAs using the solvatochromic dye Nile Red.[31] Adding Nile Red to the supramolecular polymers showed a λ_{max} of 612 nm for assemblies of **EG-BTA** and a λ_{max} of 628 nm for assemblies of **Glu-BTA** (Fig. S10, ESI†). Interestingly, whereas all previous results at low temperatures point towards similar morphologies for assemblies of **EG-BTA** and **Glu-BTA**, the Nile Red experiments suggest structural variances between the assemblies; the environment surrounding the **Glu-BTA** core is less hydrophobic as compared to that of the **EG-BTA** assemblies.

To obtain a molecular insight into the subtle hydrophobicity differences between **EG-BTA** and **Glu-BTA** and their interactions with water, we performed all atom molecular dynamics (MD) simulations on a model of supramolecular polymer of **Glu-BTA** using the same procedure applied for **EG-BTA** fibres.[32] We started from a model of an ideal fibre composed of 48 pre-stacked and initially extended **Glu-BTA** units. The atomistic model for the **Glu-BTA** fibre was built and parameterised following the same procedure used for **EG-BTA** (see ESI† for computational details).[32] The initial extended configuration for the atomistic **Glu-BTA** fibre model replicates along the main axis of a simulation box filled with explicit water molecules by means of periodic boundary conditions, effectively modelling the bulk of an infinite **Glu-BTA** supramolecular fibre (Fig. S11A, ESI†). The starting geometry of the **Glu-BTA** fibre is thus identical to that of the previously studied **EG-BTA**. This fibre was then equilibrated in water through 400 ns of MD simulation at 20 °C (see ESI† for simulation details). During this time the **Glu-BTA** fibre model reached the equilibrium in the atomistic MD regime.

During the simulations, the initially extended **Glu-BTA** fibre structurally reorganises to optimise the interactions between the monomers and with the solvent.[32] After equilibration, the **Glu-BTA** fibre side chains appear more extended than those of **EG-BTA** (Fig. S11A & S11B, ESI†). Previous MD simulations of **EG-BTA** fibres revealed that the flexible **EG-C_{12}** side chains collapse around the core of the fibre to reduce the hydrophobic area exposed to the solvent (primary folding). After this phase significant hydrophobic regions along the fibre were still in contact with water. Consequently, the **EG-BTA** fibre was seen to undergo (secondary) folding along the main fibre axis to further reduce the exposed hydrophobic area.[32] Such a secondary folding process is not observed along the MD run in case of the **Glu-BTA** fibres. This is reflected into a higher persistence/order of the core-core stacking in the equilibrated **Glu-BTA** fibre when compared to **EG-BTA**. The radial distribution functions (Fig. S11C, ESI†) demonstrate higher *g(r)* peaks at stacking distances c (= 3.4 Å), 2c, 3c, etc. The higher the *g(r)* peaks, the higher the stacking persistence, indicating a higher probability for finding cores at stacking distance in case of **Glu-BTA**.[32] In general, the **Glu-BTA** fibre deviates less from the extended fibre configuration during the MD simulation compared to the **EG-BTA** fibre (see Fig. S11).

When analysing the organisation of the glucose moieties at the surface of the fibres in more detail, numerous H-bond interactions between the glucose moieties are observed. Closer inspection of the MD trajectories shows that these H-bonds can be direct (saccharide-saccharide) or even indirect,

involving bridging by water molecules (saccharide-water-saccharide). Quantitative analysis of the H-bonding in these fibres demonstrates that the H-bonds involving glucose residues in **Glu-BTA** (either direct or indirect) are way more numerous than those between the core amides. In the case of the **Glu-BTA** fibre, the average number of H-bonds (per monomer) between the core amides (Fig. 2: green) is in the same range of those of the **EG-BTA** fibre[32] (~2.1 per monomer on average), while those between the saccharides in **Glu-BTA** (Fig. 2: purple) are about twice in number (see Table 1). Moreover, the indirect H-bonds involving bridging by water molecules in **Glu-BTA** – *i.e.*, "wet" H-bonds (Fig. 2: cyan) – are one order of magnitude more numerous than the core ones (Table 1).

The surface of the **Glu-BTA** fibre thus appears as a hydrogel-like structure, in which water molecules can be involved in H-bonding and immobilised by the glucose residues (Fig. 2). In general, the MD simulations indicate that the additional H-bond interactions between the surface glucose residues make the periphery of the fibre more hydrated compared to **EG-BTA**. This increased hydration of the periphery and core in **Glu-BTA** also matches with the increased λ_{max} reported with Nile Red experiments.

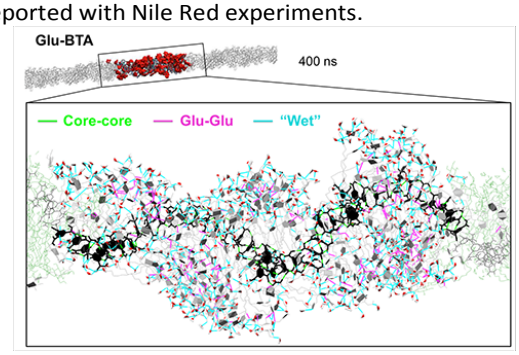

Fig. 2 Details of H-bond interactions in the equilibrated **Glu-BTA** fibre. At the MD equilibrium (400 ns), the saccharides form clusters (in red in the top image) on the fibre surface. **Glu-BTA** cores are coloured in black, side chains in grey and saccharides are shown as grey filled rings (periodic image in green). Core-core hydrogen bonds through the amides are coloured in green, saccharide-saccharide direct H-bonds in purple and indirect ones involving water molecules (red and white) in cyan.

Table 1. Average number of H-bonds per-monomer calculated from the equilibrated phase MD simulations (last 100 ns).

Assembly	Core-core[a]	End-end[b]	Total "dry"[e]	Wet[d]
EG-BTA[32]	2.2	-	2.2	8.0
Glu-BTA	2.1	3.8	5.9	21.1

[a]Average number of H-bonds between the core amides. [b]Average number of H-bonds between the saccharides of **Glu-BTA** or the TEG terminal units of **EG-BTA**. [c]Sum of the core-core and end-end H-bonds. [d]Average number of H-bonds with water molecules.

To evaluate if the exchange of BTA monomers between different fibres is affected by a better hydration of the peripheral groups, we conducted HDX-MS on **Glu-BTA** and compared the results to those of **EG-BTA**. With HDX-MS, the exchange of labile hydrogens for deuteriums from the surrounding D_2O is probed as a function of time. Both access of D_2O to the core amides within the fibres as well as the exchange of monomers between fibres may contribute to the H/D exchange rate. First, we confirm with UV-Vis that diluting a sample of **Glu-BTA** 100 times does not influence the morphology of the assemblies (Fig. S12, ESI†). **Glu-BTA** has 15 labile hydrogens, 12 OH of the glucose and 3 NH of the amide core, which can be exchanged for deuteriums during the HDX process. The ESI-MS spectrum of **Glu-BTA** taken 1 h after diluting the sample into D_2O, shows more than one isotope distribution (Fig. S13B, ESI†): one corresponding to BTAs with only the alcohol hydrogens exchanged (**Glu-BTA12D**) and one corresponding to all labile hydrogens exchanged for deuteriums (**Glu-BTA15D**). This clearly indicates that not all amide hydrogens are exchanged. As a reference, the ESI-MS spectrum was recorded in the presence of acetonitrile (Fig. S13A, ESI†), in which the BTAs are molecularly dissolved. In this case, only an isotope distribution corresponding to **Glu-BTA15D** was found. After 3 days of H/D exchange in D_2O the intensity of the peak corresponding to **Glu-BTA15D** has increased at the expense of the peak corresponding to **Glu-BTA12D** (Fig. S13C, ESI†), suggesting that more BTAs became accessible to the solvent.

In addition, the percentage of BTAs with non-exchanged amide hydrogens was plotted as a function of time (**BTA-3NH** in Fig. 3, corresponding to **EG-BTA3D** and **Glu-BTA12D**). After 72 hours, 24% of **EG-BTA3D** and 13% for **Glu-BTA12D** is present, indicating that for the latter more BTAs exchanged all labile hydrogens with D_2O. Globally, this suggests that the BTA amides are less shielded from D_2O in fibres of **Glu-BTA** as compared to **EG-BTA**. In addition, the decay curve in Fig. 3 of **Glu-BTA** was fitted to a tri-exponential decay, in which a very fast, initial exchange process, a fast, and a slow one are distinguished.[24] The three exchange processes are quantified by both a rate constant as well as a relative contribution of each of the HDX processes (Table 2). Comparing the rate constants of each of the three processes for both fibre types shows that $k_{initial}$ and k_{fast} are higher for **Glu-BTA**, contributing to a faster initial exchange of **Glu-BTA** monomers (Fig. S14, ESI†). In contrast, the slow process shows a lower rate constant k_{slow} and contributes significantly less in case of **Glu-BTA**. Analysis of the percentage of BTAs with only one or two amide hydrogens exchanged for deuteriums permits a better understanding of the origin of the H/D exchange (Fig. S15, ESI†). If individual D_2O molecules access the BTA amides inside the fibres, H/D exchange will occur one single amide-NH at a time, whereas the release of a single BTA molecule from the fibre would exchange all three amide-NH to amide-NDs at the same time. In both assemblies, a small percentage of amide-1ND and amide-2ND is observed during the first 60 min of the HDX experiment (see Fig. S15, ESI†). The presence of these intermediate populations indicates that the accessibility of the amides to D_2O molecules contributes to the H/D exchange in the early stages. At later stages of the HDX process, only amide-3NH and amide-3NDs are observed, indicating that H/D exchange is dominated by monomer exchange between fibres. The lower k_{slow} for **Glu-BTA** suggests that monomer exchange occurs slower, and indicates that the fibres are more static in terms of exchange of monomers. In contrast, the higher values for $k_{initial}$ and k_{fast} in case of **Glu-BTA** may be related to the

water hydration layer around the saccharides. The exact origin of rigidity of the fibres over time is currently unclear and topic of further investigations.

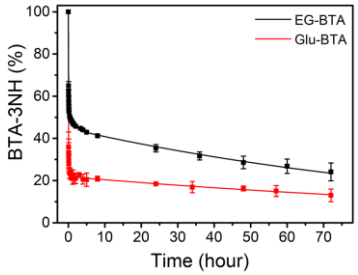

Fig. 3 The percentage of BTAs with non-exchanged amide hydrogens (BTA-3NH) for **EG-BTA** (black) and **Glu-BTA** (red) assemblies as a function of time after diluting a 500 μM BTA solution 100 times into D_2O, at room temperature. The squares represent the average percentage and the error bars represent the standard deviation both calculated from three independent measurements. All data was fitted to a tri-exponential fit.

Table 2. Rate constants, *k*, and relative contributions of the H/D exchange process as obtained from the tri-exponential fitting of the data in Fig. 3.

	Rate constants (h^{-1})			Contributions (%)		
	$k_{initial}$	k_{fast}	k_{slow}	Initial	Fast	Slow
EG-BTA	25	0.79	8.9×10^{-3}	47.0	8.3	44.7
Glu-BTA	70	6.6	6.9×10^{-3}	61.0	17.2	21.8

In summary, supramolecular building blocks with saccharides as the water-compatible periphery form supramolecular polymers in aqueous solution at 20 °C with morphologies and dimensions that appear at first very similar to those previously reported for supramolecular motifs with TEG chains, but possess a less hydrophobic interior. In addition, a higher extent of H/D exchange was observed on short time scales whereas the fibres are more static in terms of exchange of monomers on longer time scales compared to **EG-BTA**. MD-simulations reveal that the surface saccharides of **Glu-BTA** are more exposed on the fibre surface and that there are numerous H-bonding interactions between the saccharides, both direct and through bridging by water molecules. This research not only emphasizes the importance of a careful consideration when designing the periphery of a supramolecular motif, but it also opens the door to multivalent, water-compatible supramolecular polymers for biological recognition.

Acknowledgments

This work was supported by the Dutch Ministry of Education, Culture and Science (Gravity program 024.001.035). GMP acknowledges the support from the Swiss National Science Foundation (SNSF grant 200021_162827). Jolanda Spiering is gratefully acknowledged for synthetic support.

Notes and references

1 V. M. Dembitsky, *Chem. Biodivers.*, 2004, **1**, 673–781.
2 M. Delbianco, P. Bharate, S. Varela-Aramburu and P. H. Seeberger, *Chem. Rev.*, 2016, **116**, 1693–1752.
3 I. Papp, J. Dernedde, S. Enders, S. B. Riese, T. C. Shiao, R. Roy and R. Haag, *ChemBioChem*, 2011, **12**, 1075–1083.
4 C. R. Becer, M. I. Gibson, J. Geng, R. Ilyas, R. Wallis, D. A. Mitchell and D. M. Haddleton, *J. Am. Chem. Soc.*, 2010, **132**, 15130–15132.
5 M. J. Joralemon, K. S. Murthy, E. E. Remsen, M. L. Becker and K. L. Wooley, *Biomacromolecules*, 2004, **5**, 903–913.
6 Y. B. Lim, S. Park, E. Lee, H. Jeong, J. H. Ryu, M. S. Lee and M. Lee, *Biomacromolecules*, 2007, **8**, 1404–1408.
7 B. Bondurant, J. A. Last, T. A. Waggoner, A. Slade and D. Y. Sasaki, *Langmuir*, 2003, **19**, 1829–1837.
8 N. Nagahori, R. T. Lee, S. I. Nishimura, D. Pagé, R. Roy and Y. C. Lee, *ChemBioChem*, 2002, **3**, 836–844.
9 D. Straßburger, N. Stergiou, M. Urschbach, H. Yurugi, D. Spitzer, D. Schollmeyer, E. Schmitt and P. Besenius, *ChemBioChem*, 2018, 10–15.
10 D. Grünstein, M. Maglinao, R. Kikkeri, M. Collot, K. Barylyuk, B. Lepenies, F. Kamena, R. Zenobi and P. H. Seeberger, *J. Am. Chem. Soc.*, 2011, **133**, 13957–13966.
11 M. J. Clemente, P. Romero, J. L. Serrano, J. Fitremann and L. Oriol, *Chem. Mater.*, 2012, **24**, 3847–3858.
12 Z. Yang, G. Liang, M. Ma, A. S. Abbah, W. W. Lu and B. Xu, *Chem. Commun.*, 2007, 843–845.
13 Y. Ogawa, C. Yoshiyama and T. Kitaoka, *Langmuir*, 2012, **28**, 4404–4412.
14 K. Petkau-Milroy, M. H. Sonntag and L. Brunsveld, *Chem. - A Eur. J.*, 2013, **19**, 10786–10793.
15 E. Krieg, M. M. C. Bastings, P. Besenius and B. Rybtchinski, *Chem. Rev.*, 2016, **116**, 2414–2477.
16 J. H. Ortony, C. J. Newcomb, J. B. Matson, L. C. Palmer, P. E. Doan, B. M. Hoffman and S. I. Stupp, *Nat. Mater.*, 2014, **13**, 812–816.
17 L. H. Beun, L. Albertazzi, D. Van Der Zwaag, R. De Vries and M. A. Cohen Stuart, *ACS Nano*, 2016, **10**, 4973–4980.
18 S. Swaminathan, C. Fowley, B. McCaughan, J. Cusido, J. F. Callan and F. M. Raymo, *J. Am. Chem. Soc.*, 2014, **136**, 7907–7913.
19 N. M. Casellas, S. Pujals, D. Bochicchio, G. M. Pavan, T. Torres, L. Albertazzi and M. García-Iglesias, *Chem. Commun.*, 2018, **54**, 4112–4115.
20 N. Zweep, A. Hopkinson, A. Meetsma, W. R. Browne, B. L. Feringa and J. H. Van Esch, *Langmuir*, 2009, **25**, 8802–8809.
21 K. Venkata Rao, D. Miyajima, A. Nihonyanagi and T. Aida, *Nat. Chem.*, 2017, **9**, 1133–1139.
22 F. Aparicio, F. García and L. Sánchez, *Chem. - A Eur. J.*, 2013, **19**, 3239–3248.
23 K. Petkau-Milroy, D. A. Uhlenheuer, A. J. H. Spiering, J. A. J. M. Vekemans and L. Brunsveld, *Chem. Sci.*, 2013, **4**, 2886.
24 X. Lou, R. P. M. Lafleur, C. M. A. Leenders, S. M. C. Schoenmakers, N. M. Matsumoto, M. B. Baker, J. L. J. van Dongen, A. R. A. Palmans and E. W. Meijer, *Nat. Commun.*, 2017, **8**.
25 C. M. A. Leenders, L. Albertazzi, T. Mes, M. M. E. Koenigs, A. R. A. Palmans and E. W. Meijer, *Chem. Commun.*, 2013, **49**, 1963.
26 K. Knop, R. Hoogenboom, D. Fischer and U. S. Schubert, *Angew. Chemie - Int. Ed.*, 2010, **49**, 6288–6308.
27 C. M. A. Leenders, G. Jansen, M. M. M. Frissen, R. P. M. Lafleur, I. K. Voets, A. R. A. Palmans and E. W. Meijer, *Chem. - A Eur. J.*, 2016, **22**, 4608–4615.
28 G. Vancoillie, D. Frank and R. Hoogenboom, *Prog. Polym. Sci.*, 2014, **39**, 1074–1095.
29 M. B. Baker, L. Albertazzi, I. K. Voets, C. M. A. Leenders, A. R. A. Palmans, G. M. Pavan and E. W. Meijer, *Nat. Commun.*, 2015, **6**, 6234.
30 L. N. Neumann, M. B. Baker, C. M. A. Leenders, I. K. Voets, R. P. M. Lafleur, A. R. A. Palmans and E. W. Meijer, *Org. Biomol. Chem.*, 2015, **13**, 7711–7719.
31 M. C. A. Stuart, J. C. Van De Pas and J. B. F. N. Engberts, *J. Phys. Org. Chem.*, 2005, **18**, 929–934.
32 M. Garzoni, M. B. Baker, C. M. A. Leenders, I. K. Voets, L. Albertazzi, A. R. A. Palmans, E. W. Meijer and G. M. Pavan, *J. Am. Chem. Soc.*, 2016, **138**, 13985–13995.

Table of content image:

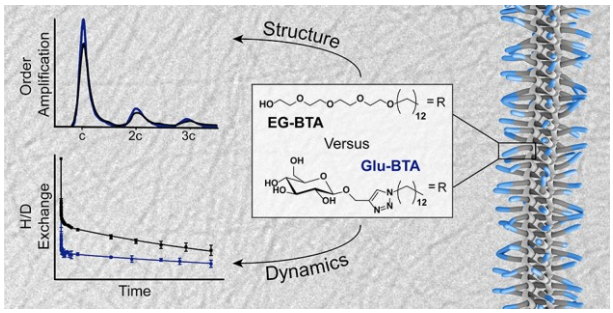

Similar morphologies but a different dynamic behaviour are revealed for supramolecular polymers in water differing in their water-compatible periphery